Appl. Phys. A (2005)
DOI: 10.1007/s00339-005-3294-1
Applied Physics A
Materials Science & Processing

Y. QU[1,2,✉]
J.X. ZHANG[2]
A. UDDIN[2]
C.Y. LIU[2]
S. YUAN[3]
M.C.Y. CHAN[4]
B. BO[1]
G. LIU[1]
H. JIANG[1]

Temperature dependence of interband transition energy in InGaAsN strain-compensated quantum-well and ridge-waveguide lasers fabricated with pulsed anodic oxidation

[1] National Key Laboratory of High Power Semiconductor Lasers, Changchun University of Science and Technology, No. 7089 Weixing Road, Changchun 130022, P.R. China
[2] School of Materials Engineering, Nanyang Technological University, 639798, Singapore
[3] Ting Gi Technologies, 83 Science Park Drive, 118258, Singapore
[4] Department of Electrical and Electronic Engineering, The University of Hong Kong, Hong Kong, P.R. China

Received: 4 April 2005/Accepted: 2 May 2005
Published online: 28 June 2005 • **© Springer-Verlag 2005**

ABSTRACT Ridge-waveguide InGaAsN triple-quantum-well strain-compensated lasers grown by metal organic chemical vapor deposition were fabricated with pulsed anodic oxidation. The laser's output power reached 145 mW in continuous-wave mode at room temperature for a 4-μm-stripe-width laser. Continuous-wave single longitudinal mode operation was maintained at a high injection current level with a wavelength of 1287.3 nm at room temperature. Single longitudinal mode operation at 1317.2 nm was achieved at twice the threshold current at 100 °C. The band gap of InGaAsN in the quantum wells at different temperatures was calculated and compared to the measured temperature-dependent laser wavelength.

PACS 78.55.Cr; 78.67.De; 81.15.Gh; 42.55.Px

1 Introduction

Semiconductor lasers at wavelengths around 1.3 μm are widely used for fiber optic communications [1]. InGaAsP/ InP lasers are currently used for optical access and interconnection systems, but these lasers exhibit a relatively low characteristic temperature (T_0) due to poor electron confinement [2]. The incorporation of nitrogen into InGaAs reduces the band-gap energy and allows emission wavelengths as long as 1.3 μm [3–7]; this makes it possible to fabricate low-cost, long-wavelength vertical cavity surface emitting lasers (VCSELs) on GaAs substrates. InGaAsN lasers also have a higher characteristic temperature than InGaAsP lasers [3].

The performance of InGaAsN lasers significantly depends on the laser structure and material quality. Normally, high nitrogen content reduces the radiative recombination efficiency. Therefore, higher indium content is used with lower nitrogen content to reach the desired wavelength ∼ 1.3 μm and emission efficiency. However, a high indium content causes a higher strain in the quantum-well (QW) structure. A thin critical-layer thickness, and a limited number of quantum wells, are used in the active region. The use of strain-compensated barriers in the active region helps to reduce these constraints [8–12]. However, despite considerable effort the device performance in InGaAsN quantum wells is not yet satisfactory.

In addition to material quality, the laser performance can also be further improved in the fabrication processes. A uniform and high-quality, current-blocking layer is a critical component in the fabrication of semiconductor lasers. This layer is usually deposited by plasma enhanced chemical vapor deposition (PECVD). The fabrication process is relatively costly and complicated. The pulsed anodic oxidation (PAO) process is a simple and cost-effective method for the fabrication of optoelectronic devices [13]. It is also a self-alignment process. The PAO process involves only one photolithography step for the selective oxidation. Previously, PAO was applied to quantum-well intermixing in GaAs/AlGaAs and InGaAs/GaAs quantum-well and quantum-wire structures [14]. Recently, we have also reported a significant reduction of threshold-current density in InGaAsN QW lasers fabricated with a PAO system [15, 16].

In this work, the PAO process was used to improve the performance of ridge-waveguide InGaAsN lasers. We calculated the interband transition energy in the quantum well as a function of temperature to quantify the temperature dependence of the laser wavelength. However, the laser wavelength does not actually correspond to the interband transition energy, but is rather determined by the gain spectrum of the laser wafer and the laser cavity modes. The temperature dependence of the interband transition energy does provide useful information and should follow the same trend.

2 Experiment

The wafer used in this work was grown by a metal organic chemical vapor deposition (MOCVD) system. The wafer structure is listed in Table 1. The active region consists of three $In_{0.35}Ga_{0.65}As_{0.985}N_{0.015}$ quantum wells (QWs), each QW 6.4-nm thick, separated by 7-nm GaAs and 8-nm $GaAs_{0.82}P_{0.18}$ barrier layers. The active region was symmetrically embedded in a 35-nm-thick undoped GaAs wave-

✉ Fax: +86-431-5384517, E-mail: yiqu@public.cc.jl.cn

Layer	Remarks	Thickness (nm)	Doping ($1/cm^3$)
GaAs	Contact layer	200	C, 1.4×10^{19}
$Al_xGa_{1-x}As$	$x = 0.5$–0	100	C, 5×10^{17}
$Al_{0.5}Ga_{0.5}As$		900	C, 5×10^{17}
$Al_xGa_{1-x}As$	$x = 0$–0.5	200	Undoped
GaAs		35	Undoped
$GaAs_{0.82}P_{0.18}$		12	Undoped
GaAs		7	Undoped
$In_{0.35}Ga_{0.65}As_{0.985}N_{0.015}$		6.4	Quantum well
GaAs		7	Undoped
$GaAs_{0.82}P_{0.18}$		8	Undoped
GaAs		7	Undoped
$In_{0.35}Ga_{0.65}As_{0.985}N_{0.015}$		6.4	Quantum well
GaAs		7	Undoped
$GaAs_{0.82}P_{0.18}$		8	Undoped
GaAs		7	Undoped
$In_{0.35}Ga_{0.65}As_{0.985}N_{0.015}$		6.4	Quantum well
GaAs		7	Undoped
$GaAs_{0.82}P_{0.18}$		12	Undoped
GaAs		35	Undoped
$Al_xGa_{1-x}As$	$x = 0.5$–0	200	Undoped
$Al_{0.5}Ga_{0.5}As$		900	Si, 6×10^{17}
$Al_xGa_{1-x}As$	$x = 0$–0.5	100	Si, 5×10^{17}
GaAs	Buffer layer	200	Si, 1×10^{18}
(100) GaAs	Substrate		Si, 1×10^{18}

TABLE 1 Wafer structure of the InGaAsN strain-compensated triple-quantum-well lasers

guide. A 1.2-μm-thick Si-doped ($6 \times 10^{17}\,cm^{-3}$) n-type $Al_xGa_{1-x}As$ ($x = 0$–0.5) cladding layer was grown between the n-substrate and the active layer. A 1.2-μm-thick C-doped ($5 \times 10^{17}\,cm^{-3}$) p-type $Al_xGa_{1-x}As$ ($x = 0$–0.5) cladding layer followed the active layer. A 20-nm-thick p^+ ($1 \times 10^{19}\,cm^{-3}$) GaAs cap layer was grown for ohmic contact.

Photoluminescence (PL) measurements were performed at 77 K and room temperature (20 °C) to find the band-gap energy of a QW. An argon-ion laser beam (the 514.5-nm line), a spectrometer, and a thermo-electrically cooled InGaAs detector connected to a lock-in amplifier were used for the PL measurement.

The PL spectra of the laser structure are shown in Fig. 1. The full width at half-maximum (FWHM) of 27.3 meV at 77 K and 66 meV at room temperature indicates the wafer quality.

After wafer cleaning, 4-μm photoresist stripes were first patterned by standard photolithography. Then, the mesa was etched in a solution of phosphoric acid, hydrogen peroxide, and deionized water. With the photoresist still on the ridges, pulsed anodization was performed to form the current-blocking oxide layer. The initial current density was set to $120\,mA/cm^2$ for the oxidation. The voltage-pulse duration was 1 ms, the period was 12 ms, and the total anodization time was 4 min. Figure 2 shows a typical cross-sectional scanning electron microscopy (SEM) image of the InGaAsN laser fabricated with pulsed anodic oxidation.

The wafer was thinned to ~ 100-μm thick. Ti/Au and Au–Ge/Ni/Au layers were deposited by electron-beam evaporation on the p-type and n-type sides, respectively, and annealed to make the ohmic contacts. 1600 μm cavity length laser bars were then cleaved and individual lasers were sawn. The laser chips were bonded as p-side-down onto copper heat sinks with indium [17].

The lasers were tested without facet coating in continuous-wave (cw) mode. Output power versus injection current (P–I) characterization of the laser was performed by using a calibrated InGaAs detector mounted in an integration sphere. The laser was bonded on a copper-block heat sink and placed right at the entrance of the integration sphere. The laser emission spectra were measured in cw mode by using a spectrometer, a Ge detector (cooled to –20 °C), and a data-acquisition system. The resolution of the spectrometer was 0.025 nm. The temperature of the laser was varied by a thermo-electric heater from room temperature (20 °C) to 100 °C.

3 Results and discussion

The room-temperature cw P–I characteristic of a 4 μm × 1600 μm triple-quantum-well laser is shown in Fig. 3. We stopped the measurement when the laser power reached 145 mW. The maximum slope efficiency was 0.36 W/A in the linear P–I region. Single longitudinal mode operation was observed for output powers up to 46 mW,

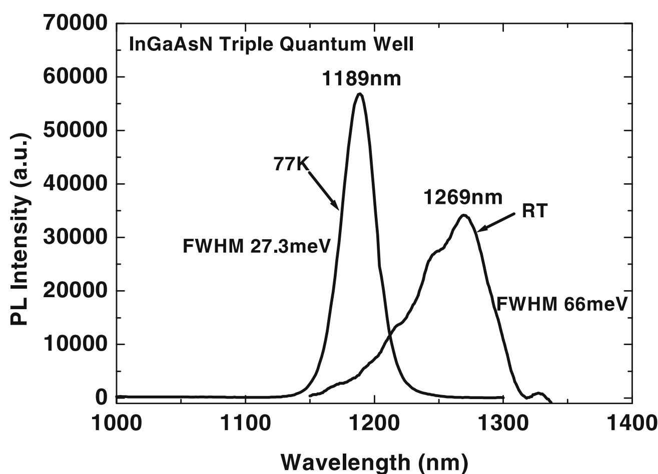

FIGURE 1 Photoluminescence spectra of InGaAsN triple-quantum-well laser structure at 77 K and room temperature (RT)

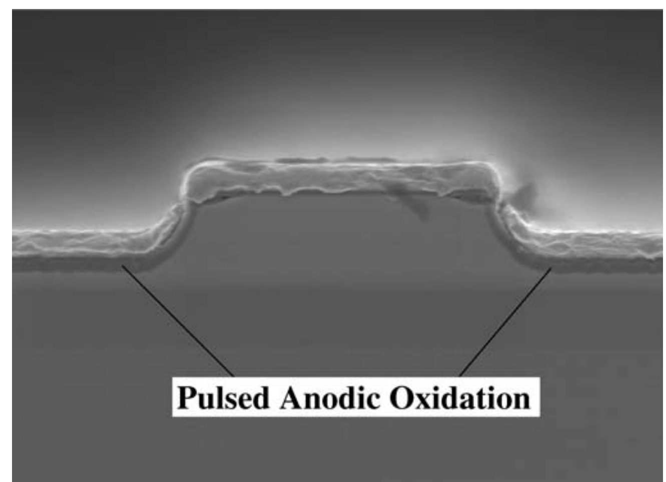

FIGURE 2 SEM image of the ridge-waveguide laser structure fabricated with pulsed anodic oxidation system

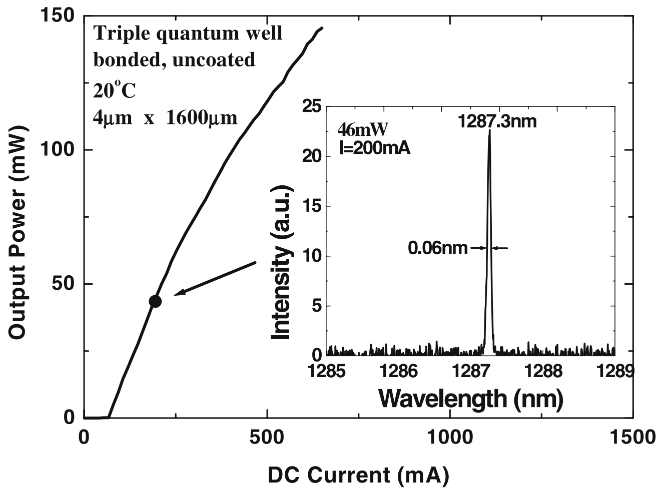

FIGURE 3 Room-temperature cw light output power versus injection current for a 4×1600 μm ridge-waveguide InGaAsN laser diode fabricated with pulsed anodic oxidation. Single-mode operation was maintained for laser power up to 46 mW. The *inset* shows the lasing spectrum at an injection current of 200 mA (46 mW). The lasers were not facet-coated, but were bonded p-side down on copper heat sinks with indium

as shown in the inset of Fig. 3. The FWHM was only 0.06 nm. The emission wavelength at a current of 200 mA was 1287.3 nm. We also measured the emission spectra of the lasers in cw mode at high temperatures up to 100 °C, and observed single longitudinal mode emission. A typical high-temperature (100 °C) spectrum from the 4-μm-stripe laser is shown in Fig. 4, with an emission wavelength of 1317.2 nm. The output power of the device was up to 5 mW.

As a comparison, lasers were fabricated by a conventional method, where the current-blocking layer was SiO_2 deposited by a PECVD instead of a PAO process [18]. The wafer was from the same wafer as used in this work. The ridge width was 2 μm and the laser cavity lengths were 400 μm. The devices were soldered p-side up onto a Si carrier tile and uncoated. The threshold-current density was 1.95 kA/cm^2. The maximum cw output power was 18 mW from the laser. The

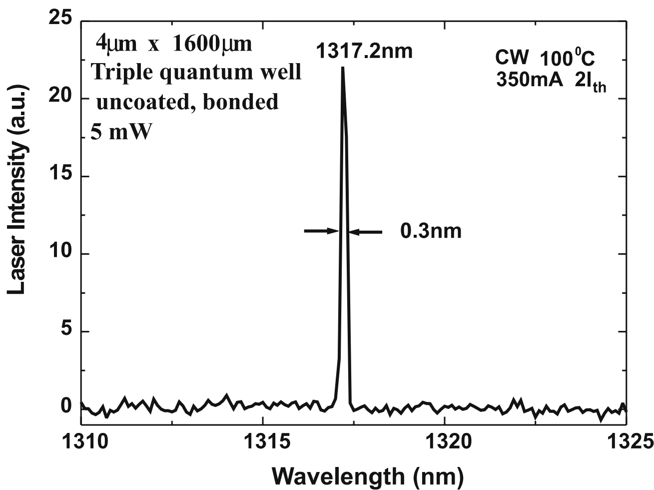

FIGURE 4 Lasing spectrum of the 4-μm-stripe-width InGaAsN triple-quantum-well laser at 100 °C

lasers were also fabricated by the same conventional method (2-μm stripe width, 400-μm cavity length) from the three-quantum-well wafer without strain-compensated GaAsP barriers [18]. The threshold-current density was 2.2 kA/cm^2. The maximum cw output power was 12 mW from the laser. A laser fabricated with PAO with a ridge width of 4 μm and a cavity length of 400 μm showed a threshold-current density of 1.25 kA/cm^2. These PAO lasers were also unbonded and uncoated, and were tested in cw mode. The maximum power was 40 mW in a 400-μm-long laser. It should be pointed out that ridge-waveguide lasers with narrower ridge width usually show higher threshold-current density and lower output power, due to high lateral current leakage and smaller active volume [19].

The material parameters of GaAs, GaN, InAs, and InN at room temperature are given in Table 2. The temperature-dependent energy gaps of binary alloys GaAs, GaN, InAs, and InN is given by the Varshni relation [20]

$$E_g(T) = E_g(T=0) - \frac{\alpha T^2}{T+\beta}, \tag{1}$$

where α and β are constants and their values are listed in Table 2.

The calculated temperature-dependent interband transition energy of the InGaAsN triple-quantum-well laser and the measured lasing wavelength of the laser are shown in Fig. 5. The emission-wavelength shift with temperature was 0.42 nm/°C, which was affected by the temperature dependence of the band gap (0.54 nm/°C). When the temperature was increased, the emission wavelength was linearly increased.

For comparison, the room-temperature PL peak wavelength is also shown in Fig. 5, which agrees with the calculated interband transition energy. According to previous studies [29], carriers are localized at low temperature (<

	GaAs	GaN	InAs	InN	Units
a_0	5.6533[a]	4.46[b]	6.0583[a]	5.02[d]	Å
c_{11}	11.9[a]	29.6[b]	8.329[a]	18.4[c]	$\times 10^{11}$ dyn/cm^2
c_{12}	5.38[a]	15.4[b]	4.526[a]	11.6[d]	$\times 10^{11}$ dyn/cm^2
dE_g/dP	11.3[a]	32.0[b]	10.2[a]	22.0[f]	$\times 10^{-6}$ eV/bar
b	−1.7[a]	−2.67[b]	−1.8[a]	−2.67[b]	eV
m_c	0.0632[a]	0.13[b]	0.0213[a]	0.14[g]	M_0
m_{hh}	0.5[a]	0.806[b]	0.517[a]	0.8[g]	M_0
m_{lh}	0.088[a]	0.205[b]	0.024[a]	0.19[g]	M_0
Δ_o	0.34[a]	0.011[b]	0.41[a]	0.006[g]	eV
$E_g(T=0\,K)$	1.519[a]	3.3[b]	0.42[a]	1.94[e]	eV
α	0.5405[a]	0.593[h]	0.25[a]	0.245[h]	meV/K
β	204[a]	600[h]	75[a]	624[h]	K

[a]Reference [21];
[b]Reference [22];
[c]Reference [23];
[d]Reference [24];
[e]Reference [25];
[f]Reference [26];
[g]Reference [27];
[h]Reference [28]

TABLE 2 The room-temperature material parameters of GaAs, GaN, InAs, and InN used in the numerical calculations

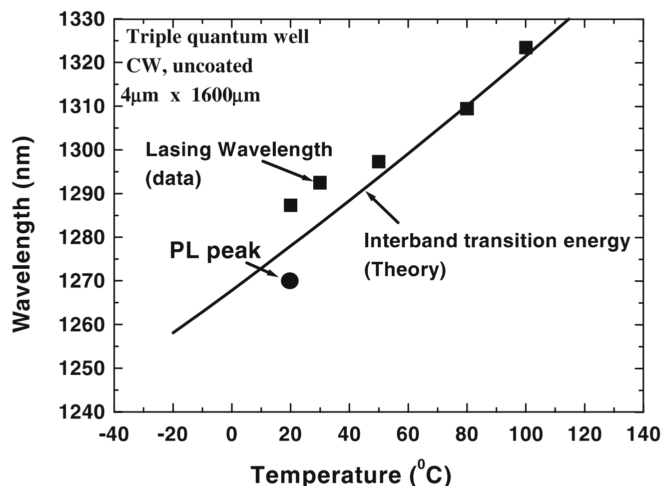

FIGURE 5 The calculated interband transition energy (*solid line*) of the InGaAsN triple-quantum-well laser and temperature-dependent lasing wavelength of 4×1600 μm InGaAsN triple-quantum-well laser. For comparison, the room-temperature PL peak wavelength is also shown

90 K). An S-shaped temperature dependence is observed. From [30], the emission wavelength as a function of operating temperature is linear. From our observation, we can conclude that the relation between the transition energy and the temperature is linear within an operating temperature of 20–80 °C.

4 Conclusions

In conclusion, pulsed anodic oxidation was applied to the fabrication of ridge-waveguide InGaAsN triple-quantum-well strain-compensated lasers grown by MOCVD. Laser output power reached 145 mW in cw mode at room temperature from the 4-μm-stripe-width lasers. Continuous-wave single longitudinal mode operation of 4-μm-stripe-width lasers was maintained up to 46 mW with a wavelength of 1287.3 nm at room temperature. In addition, single longitudinal mode operation at 1317.2 nm was achieved at twice the threshold current at 100 °C. The lasing wavelength as a function of temperature was measured and simulated; a good agreement between the trends was obtained.

ACKNOWLEDGEMENTS This work was supported by National Natural Sciences Foundation of China under contracts of 60476026 and 60477010, and also by National Key Lab for High Power Semiconductor Laser of China under contract of 03ZS3603 and 04ZS3601.

REFERENCES

1. F. Koyama, D. Schlenker, T. Miyamoto, Z. Chen, A. Matsutani, T. Sakaguchi, K. Iga: Electron. Lett. **35**, 1079 (1999)
2. H. Temkin, D. Coblentz, R.A. Logan, J.P. van der Ziel, T.R. Tanbun-Ek, D. Yadvish, A.M. Sergent: Appl. Phys. Lett. **62**, 2402 (1993)
3. M. Kondow, T. Kitatani, S. Nakatsuka, M.C. Larson, K. Nakahara, Y. Yazawa, M. Okai, K. Uomi: IEEE J. Sel. Top. Quantum Electron. **3**, 719 (1997)
4. X. Yang, J.B. Heroux, M.J. Jurkovic, W.I. Wang: Appl. Phys. Lett. **76**, 795 (2000)
5. W. Li, T. Jouhti, C.S. Peng, J. Konttinen, P. Laukkanen: Appl. Phys. Lett. **79**, 3386 (2001)
6. N. Tansu, N.J. Kirsch, L.J. Mawst: Appl. Phys. Lett. **81**, 2523 (2002)
7. N. Tansu, A. Quandt, M. Kanskar, W. Mulhearn, L.J. Mawst: Appl. Phys. Lett. **83**, 18 (2003)
8. N. Tansu, J.-Y. Yeh, L.J. Mawst: Appl. Phys. Lett. **83**, 2512 (2003)
9. W. Li, J. Turpeinen, P. Melanen, P. Savolainen, P. Uusimaa, M. Pessa: Appl. Phys. Lett. **78**, 91 (2001)
10. N. Tansu, L.J. Mawst: IEEE Photon. Technol. Lett. **14**, 444 (2002)
11. T. Jouhti, C.S. Peng, E.-M. Pavelescu, J. Konttinen, L.A. Gomes, O.G. Okhotnikov, M. Pessa: IEEE J. Sel. Top. Quantum Electron. **8**, 787 (2002)
12. N. Tansu, J.-Y. Yeh, L.J. Mawst: Appl. Phys. Lett. **82**, 3008 (2003)
13. M.J. Grove, D.A. Hudson, P.S. Zory, R.J. Dalby, C.M. Harding, A. Rosenberg: J. Appl. Phys. **76**, 587 (1994)
14. S. Yuan, Y. Kim, C. Jagadish, P.T. Burke, M. Gal, J. Zhou, D.Q. Cai, D.J.H. Cockayne, R.M. Cohen: Appl. Phys. Lett. **70**, 1269 (1997)
15. Y. Qu, C. Liu, S. Yuan: Appl. Phys. Lett. **85**, 5149 (2004)
16. Y. Qu, C. Liu, S. Ma, S. Yuan, B. Bo, G. Liu, H. Jiang: IEEE Photon. Technol. Lett. **16**, 2406 (2004)
17. Y. Qu, S. Yuan, C.Y. Liu, B.X. Bo, G.J. Liu, H.L. Jiang: IEEE Photon. Technol. Lett. **16**, 389 (2004)
18. The lasers were fabricated and the data was provided by the wafer manufacturer (IQE Europe Ltd) (private communications)
19. G. Belenky, L. Shterengas, C.L. Reynolds, Jr., M.W. Focht, M.S. Hybertsen, B. Witzigmann: IEEE J. Quantum Electron. **QE-38**, 1276 (2002)
20. P. Varshni: Physica **34**, 149 (1967)
21. E.H. Li: Physica E **5**, 215 (1999)
22. S.H. Park, S.L. Chuang: J. Appl. Phys. **87**, 353 (2000)
23. S. Strite, D. Chandrasekhar, D.J. Smith, J. Sariel, H. Chen, N. Teraguchi, H. Morkoc: J. Cryst. Growth **127**, 204 (1993)
24. A.F. Wright: J. Appl. Phys. **82**, 2833 (1997)
25. K. Kim, W.R.L. Lambrecht, B. Segall: Phys. Rev. B **53**, 16 310 (1996)
26. A.T. Meney, E.P. O'Reilly, A.R. Adams: Semicond. Sci. Technol. **11**, 897 (1996)
27. V.I. Gavrilenko, R.Q. Wu: Phys. Rev. B **61**, 2632 (2000)
28. I. Vurgaftman, J.R. Meyer, L.R. Ram-Mohan: J. Appl. Phys. **89**, 5815 (2001)
29. P. Sitarek, K. Ryczko, G. Sezk, J. Misiewicz, M. Fischer, M. Reinhardt, A. Forchel: Solid State Electron. **47**, 489 (2003)
30. M. Fischer, M. Reinhardt, A. Forchel: IEEE J. Sel. Top. Quantum Electron. **7**, 149 (2001)